Published in final edited form as:
Science. 2017 October 06; 358(6359): 116–119. doi:10.1126/science.aao2825.

Fibril structure of amyloid-ß(1-42) by cryo-electron microscopy

Lothar Gremer[1,2], **Daniel Schölzel**[1,2], **Carla Schenk**[1], **Elke Reinartz**[2], **Jörg Labahn**[1,2,3], **Raimond B.G. Ravelli**[4], **Markus Tusche**[1], **Carmen Lopez-Iglesias**[4], **Wolfgang Hoyer**[1,2], **Henrike Heise**[1,2], **Dieter Willbold**[1,2,*], and **Gunnar F. Schröder**[1,5,*]

[1]Institute of Complex Systems, Structural Biochemistry (ICS-6), Forschungszentrum Jülich, 52425 Jülich, Germany [2]Institut für Physikalische Biologie, Heinrich-Heine-Universität Düsseldorf, 40225 Düsseldorf, Germany [3]Centre for Structural Systems Biology (CSSB), DESY, 22607 Hamburg, Germany [4]The Maastricht Multimodal Molecular Imaging Institute, Maastricht University, Universiteitssingel 50, 6229 ER Maastricht, The Netherlands [5]Physics Department, Heinrich-Heine-Universität Düsseldorf, 40225 Düsseldorf, Germany

Abstract

Amyloids are implicated in neurodegenerative diseases. Fibrillar aggregates of the amyloid-β protein (Aβ) are the main component of the senile plaques found in brains of Alzheimer's disease patients. We present the structure of an Aβ(1-42) fibril composed of two intertwined protofilaments determined by cryo-electron microscopy (cryo-EM) to 4.0 Å resolution, complemented by solid-state nuclear magnetic resonance (NMR) experiments. The backbone of all 42 residues and nearly all sidechains are well resolved in the EM density map, including the entire N-terminus, which is part of the cross-β structure resulting in an overall "LS"-shaped topology of individual subunits. The dimer interface protects the hydrophobic C-termini from the solvent. The unique staggering of the non-planar subunits results in markedly different fibril ends, termed "groove" and "ridge", leading to different binding pathways on both fibril ends, which has implications for fibril growth.

Amyloids are involved in various diseases, most prominently in many neurodegenerative diseases (1–3). The amyloid-β protein (Aβ) forms fibrils that further aggregate into plaques that are found in the brains of Alzheimer's disease patients (4). These fibrils are structurally highly heterogeneous (1, 5–8), which makes the production of highly ordered samples and structure determination difficult. Aβ fibrils have been described as protofilaments intertwined in a helical geometry, existing in several polymorphs, with varying width and helical pitch, different cross-section profiles and different interactions between the protofilaments (5–7, 9, 10). The local arrangement of Aβ molecules within the fibril can vary drastically between different isomorphs, with potential implications for biological activity (3). Data from solid-state NMR experiments has allowed for building models of Aβ fibrils at atomic resolution (6, 7, 11–15). Here we present the atomic structure of Aβ(1-42)

*Corresponding Authors: Gunnar F. Schröder (gu.schroeder@fz-juelich.de) +49 2461 613259; Dieter Willbold (d.willbold@fz-juelich.de) +49 2461 612100.

The authors declare no competing financial interests.

Europe PMC Funders Author Manuscripts

fibrils by cryo-EM (Figs. 1 and 2, table S1). To facilitate structure determination, we identified conditions (aqueous solution at low pH containing organic co-solvent, see (16)) that yielded a highly homogeneous sample of fibrils as shown by EM and atomic-force microscopy (AFM) (figs. S1 and S2, see (16)). The toxicity of these fibrils was indistinguishable from fibrils grown at neutral pH (fig. S3). Micrographs revealed micrometer-long unbranched fibrils, where about 90 % of the fibrils had a rather invariable diameter of about 7 nm (fig. S1). These fibrils were used in a helical reconstruction procedure to compute a three-dimensional density to 4.0 Å resolution (Figs. 1 and 2, fig. S4, see (16)). The EM data were augmented by solid-state NMR and X-ray diffraction experiments, which were performed on identically produced fibril samples of recombinant uniformly labeled [^{15}N/^{13}C]-Aβ(1-42) and show that the EM structure is representative of the sample. Full site-specific resonance assignments from 2D and 3D homo- and heteronuclear correlation spectra could be obtained by solid-state NMR for all 42 residues (Fig. 3A and B, figs. S5 – S7, and tables S2 and S3). For most amino acid residues only one set of resonances was observed, indicative of high structural homogeneity and order.

The reconstructed fibril density and the atomic model (Fig. 1) show two twisted protofilaments composed of Aβ(1-42) molecules stacked in a parallel, in-register cross-β structure. The separation between the parallel β-strands is well visible in the density (Fig. 1A and fig. S8A). The peripheral β-sheets (residues 1–9 and 11–21) are tilted with respect to the fibril axis by ~10° (Fig. 2C). Remarkably, the fibril does not show a C_2 symmetry but instead an approximate 2_1 screw symmetry with a rise of 4.67 Å, which is in excellent agreement with the strongest peak in the X-ray diffraction profile of 4.65 Å (Fig. 3C and fig. S9). Owing to this helical symmetry, the subunits are arranged in a staggered fashion (Fig. 4A). The interaction between the protofilaments is thus not true dimeric, but the subunits are stepwise shifted along the fibril axis (fig. S10). Such an arrangement has also been described recently for dimeric tau fibril structures (17).

A single Aβ(1-42) subunit forms an LS-shaped structure, in which the N-terminus is L-shaped and the C-terminus S-shaped (cf. Fig. 1D). The C-terminus (Fig. 2 and fig. S11, A and B) roughly resembles structures of a different polymorph of Aβ(1-42) determined recently by solid-state NMR (11, 13, 14) alone (fig. S12, tables S4 to S6), while the dimer interface is completely different (discussed below). In contrast to those NMR structures, the current structure shows the N-terminal part of Aβ(1-42) to be fully visible and part of the cross-β structure of the fibril. Secondary chemical shifts from our NMR experiments and the corresponding secondary structure calculation correlate well with the EM structure (cf. Fig. 3B). Although we could not assign the long-range contacts unambiguously, all NMR cross-peaks, which are not due to sequential contacts, are in agreement with the cryo-EM structure (figs. S6 and S7). Recently reported chemical shift assignments of two brain seed-derived Aβ(1–42) fibril preparations (18) differ from our chemical shifts (table S7) suggesting different polymorphs.

Three hydrophobic clusters stabilize the subunit conformation: **1)** Ala2, Val36, Phe4, Leu34, **2)** Leu17, Ile31, Phe19, and **3)** Ala30, Ile32, Met35, Val40. Because the hydrophobic clusters expand in the stacked subunits along the fibril axis, they essentially contribute to fibril structure stability (Fig. 4B).

Combined analysis of NMR and cryo-EM data suggests salt-bridges between Asp1 with Lys28, Asp7 with Arg5, and Glu11 with His6 and His13 (16). The salt-bridges of Glu11 stabilize the kink in the N-terminal part of the β-sheet around Tyr10 (fig. S8D). This structural feature has also been reported for fibrils of the Osaka mutant E22Δ of Aβ(1-40) (12). In rat and mouse, which are animal species that are known not to develop Alzheimer's disease, His13 is replaced by arginine, which possibly prevents the formation of the kink around Tyr10.

Compared with previous Aβ42 fibril structures (11, 13, 14), significant structural differences are observed in the turn region of residues 20 to 25, for example here only Phe19 but not Phe20 is facing the hydrophobic core (Fig. 2 and fig. S12). This region, which forms two of the four edges of the Aβ(1-42) fibril, contains the sites of pathogenic familial mutations of Aβ: Flemish (A21G), Arctic (E22G), Dutch (E22Q), Italian (E22K), and Iowa (D23N). Furthermore, the effect of two mutants in the N-terminus at Ala2 can now be rationalized based on the fibril structure: A2T (Icelandic) might be protective against Alzheimer's disease, because threonine is more polar than alanine and could destabilize the fibril by disrupting the hydrophobic cluster Ala2, Val36, Phe4, Leu34 (Fig. 2). In contrast, A2V is pathogenic, which could be related to the fact that valine is more hydrophobic than alanine and would strengthen the hydrophobic interaction leading to increased fibril stability.

The staggered arrangement of the subunits has direct implications for fibril growth. Each monomer that binds to a certain fibril end sees the same interface, in contrast to a true dimeric interface (in the case of a C_2 symmetry), where added monomers would alternatingly see either two identical binding sites or a curb preformed by the preceding subunit. The binding sites presented by the two fibril ends are different from each other (Figs. 4 C and D), which leads to different binding pathways with possibly different energy barriers, and likely results in polarity of amyloid fibril growth (19, 20). The binding energy however has to be identical on both ends. The subunits are not planar but instead the chain rises along the fibril axis from the N- to the C-terminus, forming grooves and curbs at the binding interface (Figs. 4 C and D). We refer to the fibril ends as "groove" and "ridge", because β-strand 27–33 forms a ridge on the surface of one end of the protofilament, and a groove on the other end. The β-strands are staggered with relation to one another in a zipper-like fashion (Fig. 4A, fig. S11C). For example, Phe4 of subunit *i* is in contact with Leu34 and Val36 from the subunit *i*-2 directly below. At both fibril ends, the binding site for addition of subunit *i* contains contributions of subunits *i*-1, *i*-2, *i*-3, *i*-4, and *i*-5, or *i*+1, *i*+2, *i*+3, *i*+4, and *i*+5, respectively, and very small, likely insignificant contributions from *i*-7 and *i*+7 (fig. S11D). Therefore five Aβ(1-42) subunits are required to provide the full interface for monomer addition. For a fragment of six subunits, the capping subunits would have the same full contact interface as those in an extended fibril. We define this structural element of six subunits as the minimal fibril unit (fig. S11D).

The protofilament interface is formed by the C-termini, in contrast to previously determined solid-state NMR structures (11, 13), where the C-termini are solvent exposed (fig. S12). The interface is hydrophobic in the core and is formed by interactions between residues Val39 and Ile41 in subunit *i* with Val39 and Ile41 in subunits *i*+1 and *i*-1 (Fig. 4B). Moreover, the N-terminus of subunit *i* is close to the C-terminus of subunit *i*-3, and the salt bridge between

Asp1 (subunit *i*), and Lys28 (subunit *i*-5) also stabilizes the interaction between the protofilaments (Figs. 2 and 4). Our structure agrees with a previously reported low-resolution cryo-EM structure of Aβ(1-42) fibrils (21), which was prepared under similar low pH conditions, but clearly differs from the polymorph observed in (9) (fig. S13A).

Our 4.0 Å structure provides detailed insight into the architecture of Aβ(1–42) amyloid fibrils and reveals a complete model with the backbone of all 42 residues and almost all sidechains visible and highly ordered. An in-depth illustration of a protofilament interface is achieved. The regular helical symmetry has direct implications for the mechanism of fibril elongation and results in distinct binding sites for monomeric Aβ, including contacts across different subunit layers. This high-resolution structure will help to understand differences in pathogenic familial mutations, the molecular mechanism underlying fibril growth and potentially suggest ways to interfere with fibril formation and growth.

Supplementary Material

Refer to Web version on PubMed Central for supplementary material.

Acknowledgements

We thank P.J. Peters for advice and helpful discussions, H. Duimel for help with sample preparation, and the M4I Division of Nanoscopy of Maastricht University for microscope access and support. The authors gratefully acknowledge the computing time granted by the JARA-HPC Vergabegremium and VSR commission on the supercomputer JURECA at Forschungszentrum Jülich. Computational support and infrastructure was provided by the „Center for Information and Media Technology“ (ZIM) at the University of Düsseldorf (Germany). The authors acknowledge access to the Jülich-Düsseldorf Biomolecular NMR Center. D.W. was supported by grants from the “Portfolio Technology and Medicine”, the “Portfolio Drug Design” and the Helmholtz-Validierungsfonds of the Impuls und Vernetzungs-Fonds der Helmholtzgemeinschaft. H.H. was supported by the Entrepreneur Foundation at the Heinrich-Heine-University of Düsseldorf and by the DFG (HE 3243/4-1). Support from an ERC consolidator grant (grant agreement No 726368) to W.H. is acknowledged. The 4.0 Å EM density map of the Aβ(1–42) fibril has been deposited in the Electron Microscopy Data Bank with accession code EMD-3851, the coordinates of the atomic model have been deposited in the Protein Data Bank under accession code 5OQV. The NMR data have been deposited in the BMRB under the accession number 27212.

References

1. Riek R, Eisenberg DS. The activities of amyloids from a structural perspective. Nature. 2016 Nov 10.539:227. [PubMed: 27830791]
2. Knowles TP, Vendruscolo M, Dobson CM. The amyloid state and its association with protein misfolding diseases. Nature reviews. Molecular cell biology. 2014 Jun.15:384. [PubMed: 24854788]
3. Jucker M, Walker LC. Self-propagation of pathogenic protein aggregates in neurodegenerative diseases. Nature. 2013 Sep 05.501:45. [PubMed: 24005412]
4. Selkoe DJ, Hardy J. The amyloid hypothesis of Alzheimer's disease at 25 years. EMBO Mol Med. 2016 Jun 01.8:595. [PubMed: 27025652]
5. Fändrich M, Meinhardt J, Grigorieff N. Structural polymorphism of Alzheimer Aβ and other amyloid fibrils. Prion. 2009 Apr-Jun;3:89. [PubMed: 19597329]
6. Lu JX, et al. Molecular structure of β-amyloid fibrils in Alzheimer's disease brain tissue. Cell. 2013 Sep 12.154:1257. [PubMed: 24034249]
7. Paravastu AK, Leapman RD, Yau WM, Tycko R. Molecular structural basis for polymorphism in Alzheimer's β-amyloid fibrils. Proc Natl Acad Sci U S A. 2008 Nov 25.105:18349. [PubMed: 19015532]
8. Lopez del Amo JM, et al. An Asymmetric Dimer as the Basic Subunit in Alzheimer’s Disease Amyloid β Fibrils. Angewandte Chemie International Edition. 2012; 51:6136. [PubMed: 22565601]

9. Schmidt M, et al. Peptide dimer structure in an Aβ(1–42) fibril visualized with cryo-EM. Proceedings of the National Academy of Sciences. 2015 Sep 22.112:11858.
10. Eisenberg DS, Sawaya MR. Structural Studies of Amyloid Proteins at the Molecular Level. Annual review of biochemistry. 2017 Jan 03.
11. Colvin MT, et al. Atomic Resolution Structure of Monomorphic Aβ42 Amyloid Fibrils. J Am Chem Soc. 2016 Aug 03.138:9663. [PubMed: 27355699]
12. Schütz AK, et al. Atomic-resolution three-dimensional structure of amyloid β fibrils bearing the Osaka mutation. Angew Chem Int Ed Engl. 2015 Jan 02.54:331. [PubMed: 25395337]
13. Wälti MA, et al. Atomic-resolution structure of a disease-relevant Aβ(1-42) amyloid fibril. Proc Natl Acad Sci U S A. 2016 Aug 23.113:E4976. [PubMed: 27469165]
14. Xiao Y, et al. Aβ(1-42) fibril structure illuminates self-recognition and replication of amyloid in Alzheimer's disease. Nat Struct Mol Biol. 2015 Jun.22:499. [PubMed: 25938662]
15. Luhrs T, et al. 3D structure of Alzheimer's amyloid-beta(1-42) fibrils. Proc Natl Acad Sci U S A. 2005 Nov 29.102:17342. [PubMed: 16293696]
16. Materials and Methods, and additional analyses are available as supplementary materials on Science Online
17. Fitzpatrick AWP, et al. Cryo-EM structures of tau filaments from Alzheimer's disease. Nature. 2017 Jul 13.547:185. [PubMed: 28678775]
18. Qiang W, Yau WM, Lu JX, Collinge J, Tycko R. Structural variation in amyloid-beta fibrils from Alzheimer's disease clinical subtypes. Nature. 2017 Jan 12.541:217. [PubMed: 28052060]
19. DePace AH, Weissman JS. Origins and kinetic consequences of diversity in Sup35 yeast prion fibers. Nat Struct Biol. 2002 May.9:389. [PubMed: 11938354]
20. Inoue Y, Kishimoto A, Hirao J, Yoshida M, Taguchi H. Strong growth polarity of yeast prion fiber revealed by single fiber imaging. J Biol Chem. 2001 Sep 21.276:35227. [PubMed: 11473105]
21. Zhang R, et al. Interprotofilament interactions between Alzheimer's Abeta1-42 peptides in amyloid fibrils revealed by cryoEM. Proc Natl Acad Sci U S A. 2009 Mar 24.106:4653. [PubMed: 19264960]
22. Brener O, et al. QIAD assay for quantitating a compound's efficacy in elimination of toxic Aβ oligomers. Sci Rep. 2015 Sep 23.5 13222.
23. Hohn M, et al. SPARX, a new environment for Cryo-EM image processing. Journal of structural biology. 2007 Jan.157:47. [PubMed: 16931051]
24. Tang G, et al. EMAN2: an extensible image processing suite for electron microscopy. Journal of structural biology. 2007 Jan.157:38. [PubMed: 16859925]
25. Penczek PA, et al. CTER-rapid estimation of CTF parameters with error assessment. Ultramicroscopy. 2014 May.140:9. [PubMed: 24562077]
26. Emsley P, Lohkamp B, Scott WG, Cowtan K. Features and development of Coot. Acta crystallographica. Section D, Biological crystallography. 2010 Apr.66:486. [PubMed: 20383002]
27. Adams PD, et al. PHENIX: a comprehensive Python-based system for macromolecular structure solution. Acta crystallographica. Section D, Biological crystallography. 2010 Feb.66:213. [PubMed: 20124702]
28. Afonine PV, et al. Towards automated crystallographic structure refinement with phenix.refine. Acta crystallographica. Section D, Biological crystallography. 2012 Apr.68:352. [PubMed: 22505256]
29. Echols N, et al. Graphical tools for macromolecular crystallography in PHENIX. Journal of applied crystallography. 2012 Jun 01.45:581. [PubMed: 22675231]
30. Heise H, et al. Molecular-level secondary structure, polymorphism, and dynamics of full-length alpha-synuclein fibrils studied by solid-state NMR. Proc Natl Acad Sci U S A. 2005 Nov 01.102:15871. [PubMed: 16247008]
31. Hohwy M, Rienstra CM, Jaroniec CP, Griffin RG. Fivefold symmetric homonuclear dipolar recoupling in rotating solids: Application to double quantum spectroscopy. J Chem Phys. 1999 Apr 22.110:7983.
32. Baldus M, Petkova AT, Herzfeld J, Griffin RG. Cross polarization in the tilted frame: assignment and spectral simplification in heteronuclear spin systems. Mol Phys. 1998 Dec 20.95:1197.

33. Takegoshi K, Nakamura S, Terao T. 13C-1H dipolar-assisted rotational resonance in magic-angle spinning NMR. Chemical Physics Letters. 2001; 344:631.
34. Shi C, et al. BSH-CP based 3D solid-state NMR experiments for protein resonance assignment. J Biomol NMR. 2014 May 01.59:15. 2014. [PubMed: 24584701]
35. Verel R, Ernst M, Meier BH. Adiabatic dipolar recoupling in solid-state NMR: The DREAM scheme. J Magn Reson. 2001 May.150:81. [PubMed: 11330986]
36. De Paepe G, Lewandowski JR, Loquet A, Bockmann A, Griffin RG. Proton assisted recoupling and protein structure determination. J Chem Phys. 2008 Dec 28.129
37. Fung BM, Khitrin AK, Ermolaev K. An improved broadband decoupling sequence for liquid crystals and solids. J Magn Reson. 2000 Jan.142:97. [PubMed: 10617439]
38. Delaglio F, et al. NMRpipe - a multidimensional spectral processing system based on unix pipes. J Biomol NMR. 1995 Nov.6:277. [PubMed: 8520220]
39. Skinner SP, et al. CcpNmr AnalysisAssign: a flexible platform for integrated NMR analysis. J Biomol NMR. 2016; 66:111. [PubMed: 27663422]
40. Schwarzinger S, Kroon GJA, Foss TR, Wright PE, Dyson HJ. Random coil chemical shifts in acidic 8 M urea: Implementation of random coil shift data in NMRView. J Biomol NMR. 2000; 18:43. [PubMed: 11061227]
41. Li SH, Hong M. Protonation, Tautomerization, and Rotameric Structure of Histidine: A Comprehensive Study by Magic-Angle-Spinning Solid-State NMR. Journal of the American Chemical Society. 2011 Feb.133:1534. [PubMed: 21207964]
42. Keim P, Vigna RA, Morrow JS, Marshall RC, Gurd FRN. C-13 Nuclear Magnetic-Resonance of Pentapeptides of Glycine Containing Central Residues of Serine, Threonine, Aspartic and Glutamic Acids, Asparagine, and Glutamine. Journal of Biological Chemistry. 1973; 248:7811. [PubMed: 4750428]
43. Morris KL, Serpell LC. X-ray fibre diffraction studies of amyloid fibrils. Methods in molecular biology. 2012; 849:121. [PubMed: 22528087]
44. Hammersley A. FIT2D V9.129 Reference Manual V3.1. 1998
45. Winn MD, et al. Overview of the CCP4 suite and current developments. Acta crystallographica. Section D, Biological crystallography. 2011 Apr.67:235. [PubMed: 21460441]
46. Liu J, et al. Amyloid structure exhibits polymorphism on multiple length scales in human brain tissue. Scientific reports. 2016 Sep 15.6 33079.
47. Perutz MF, Staden R, Moens L, De Baere I. Polar zippers. Current biology : CB. 1993 May 01.3:249. [PubMed: 15335744]

Europe PMC Funders Author Manuscripts

Europe PMC Funders Author Manuscripts

One Sentence Summary

A complete cryo-EM structure of an Aβ(1-42) fibril reveals a protofilament interface and a defined N-terminal region.

Europe PMC Funders Author Manuscripts

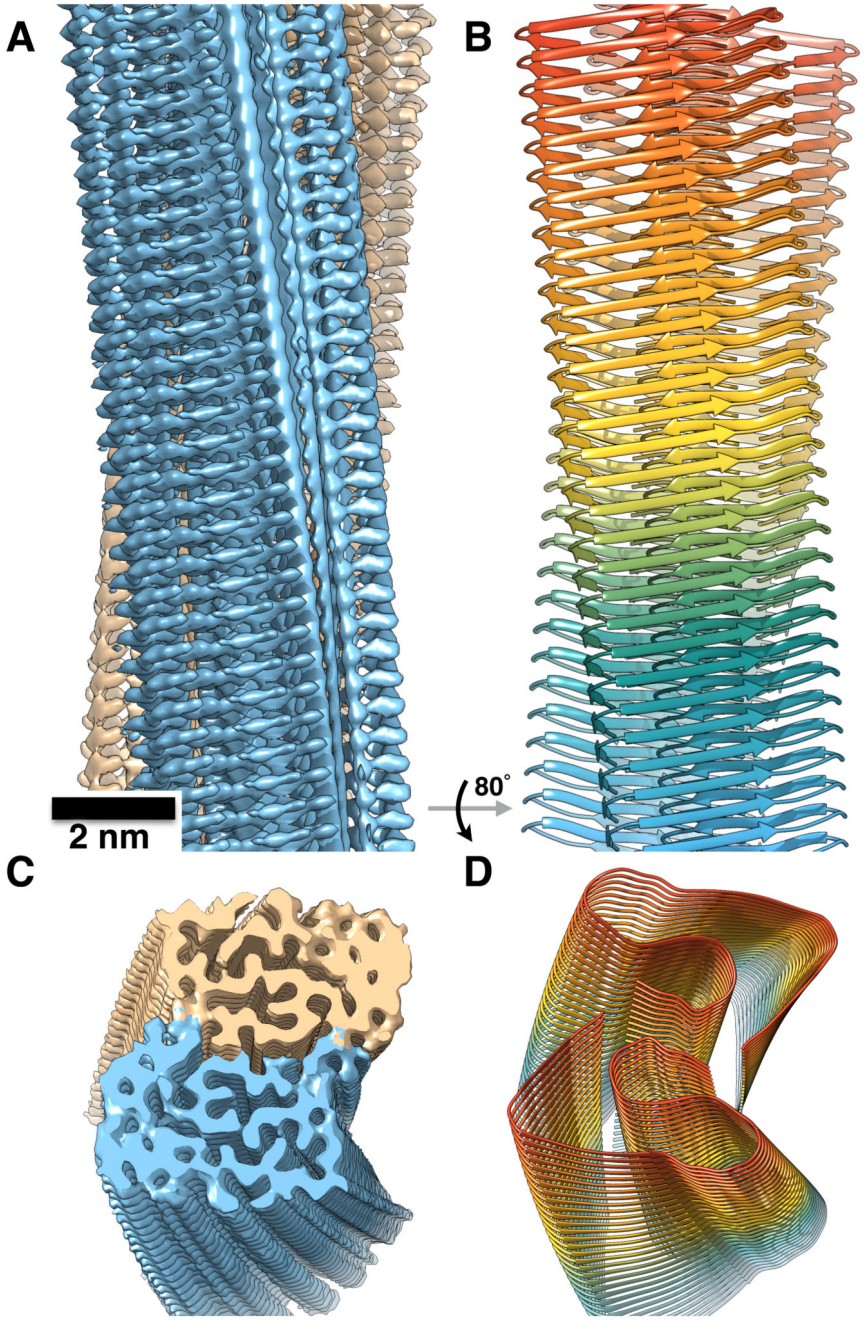

Fig. 1. Aβ(1-42) fibril structure.

(**A**) 3D reconstruction from cryo-EM images showing density of two protofilaments (brown and blue) and the clear separation of the β-strands. (**B**) Atomic model of the fibril with parallel cross-β structure. (**C**) and (**D**) Tilted views of the cross-section of the EM density and the backbone model.

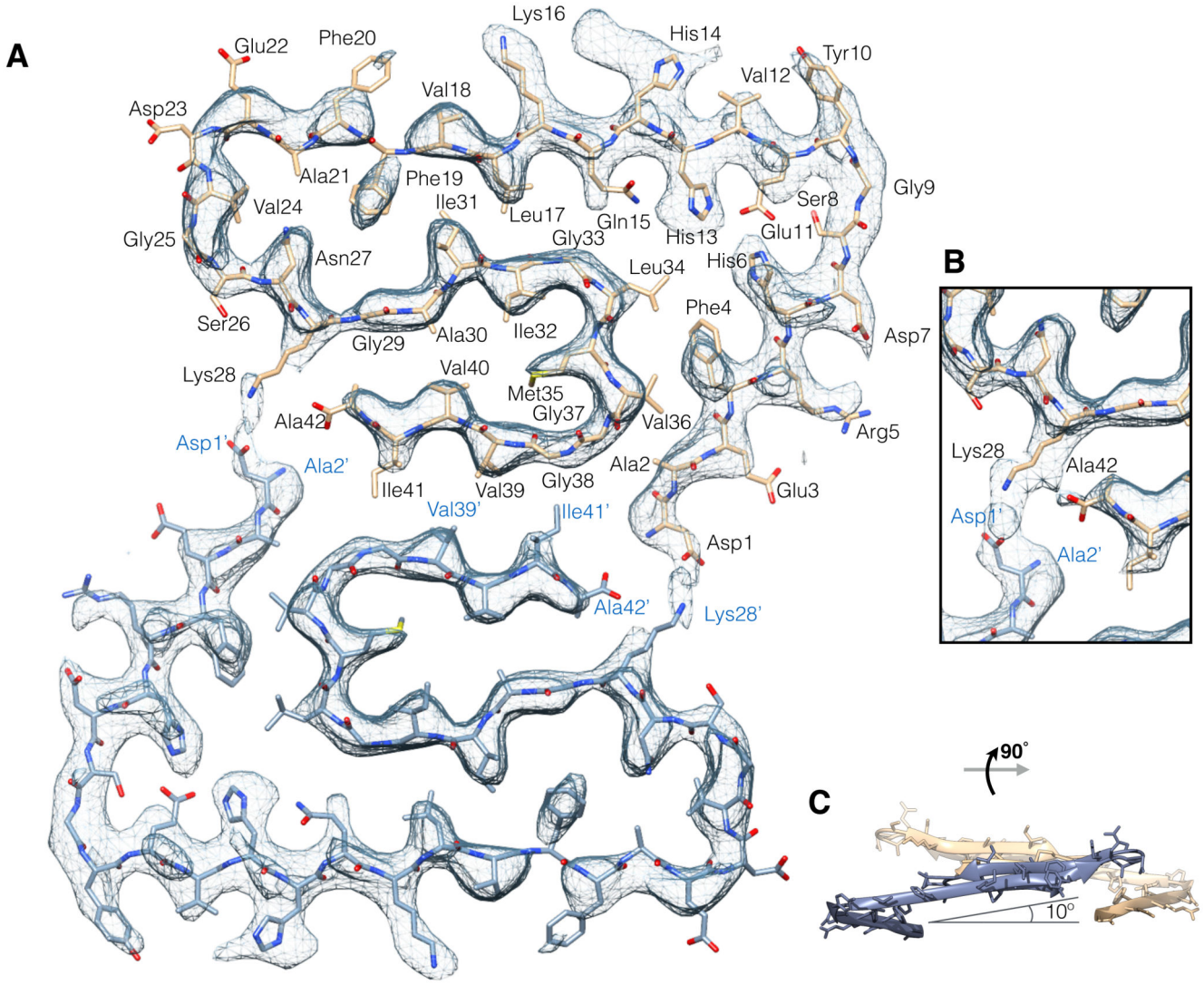

Fig. 2. Atomic model and superimposed EM density of the fibril cross-section.

(**A**) Two subunits, one from each protofilament, are shown (blue and brown) together with the masked EM density map (at contour level of 1.5 σ, additional contour levels of 1 σ and 2 σ are shown in fig. S4). (**B**) Detailed view of the interactions between the N- and C-terminus and the sidechain of Lys28 (at contour level of 1 σ). (**C**) Side view of the same two opposing subunits showing the relative orientation of the non-planar subunits. The large peripheral cross-β sheet is tilted by 10º with respect to the plane perpendicular to the fibril axis.

Europe PMC Funders Author Manuscripts

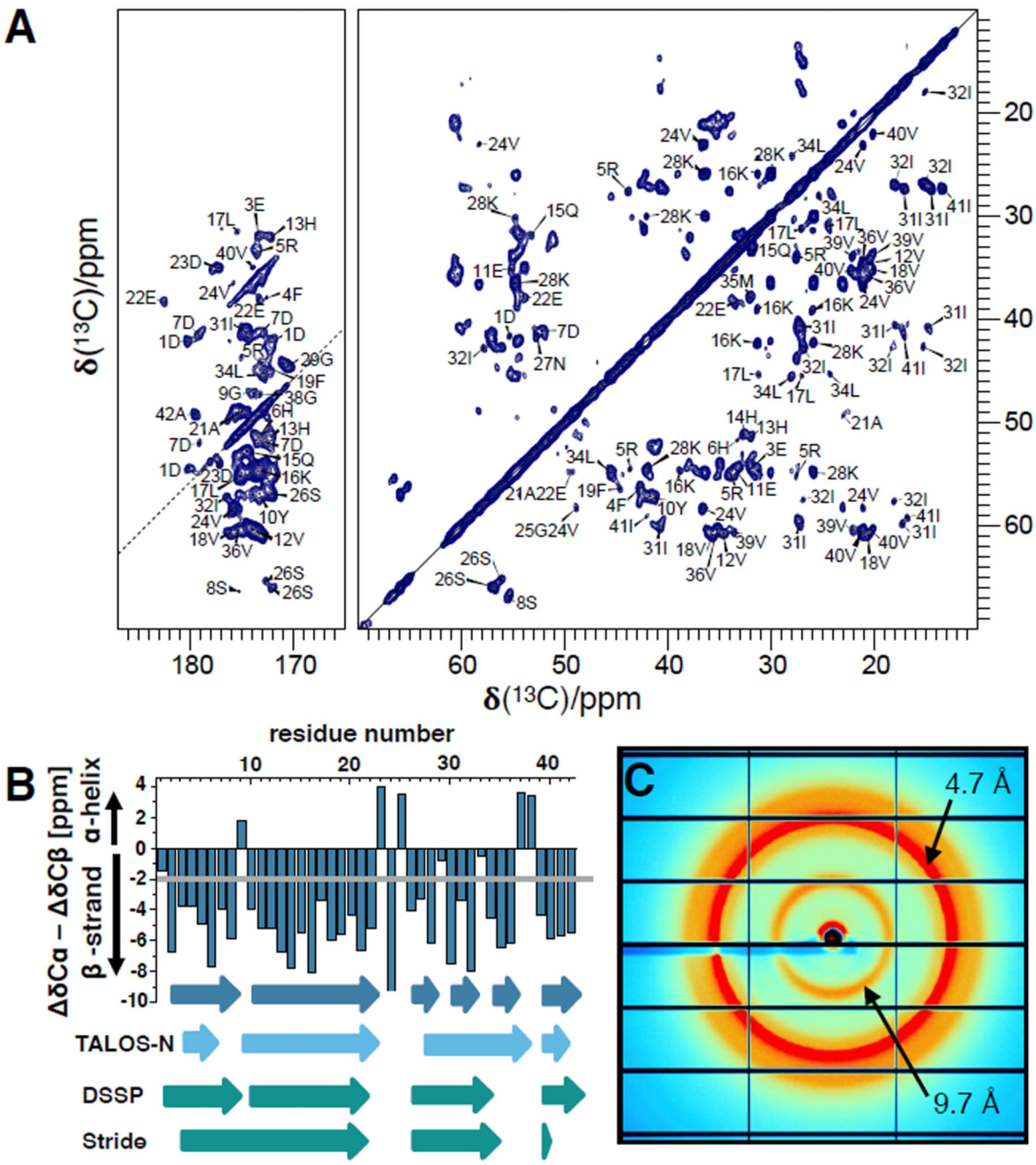

Fig. 3. NMR and X-ray diffraction experiments.

(**A**) 2D Proton-Driven Spin Diffusion (PDSD) spectrum of fibrillar Aβ(1-42). The spectrum was recorded at a magnetic field strength of 18.8 T corresponding to a proton Larmor frequency of 800 MHz, a sample temperature of T = 0 ± 5 °C and a spinning speed of 12.5 kHz. For homonuclear $^{13}C/^{13}C$ mixing, PDSD with a mixing time of 20 ms was employed. A squared and shifted sine bell function was used for apodization (shift of 0.3·π). (**B**) Secondary chemical shifts calculated from assigned resonance shifts and random coil values predicting β-strand regions (difference exceeds -2 ppm) (dark blue). For Gly residues, only

the Cα secondary chemical shifts are plotted. Additionally, β-strands calculated by TALOS-N and β-sheets from the cryo-EM derived atomic model are displayed (assigned by DSSP and Stride). (**C**) X-ray diffraction image of un-oriented Aβ(1-42) fibrils.

Europe PMC Funders Author Manuscripts

Europe PMC Funders Author Manuscripts

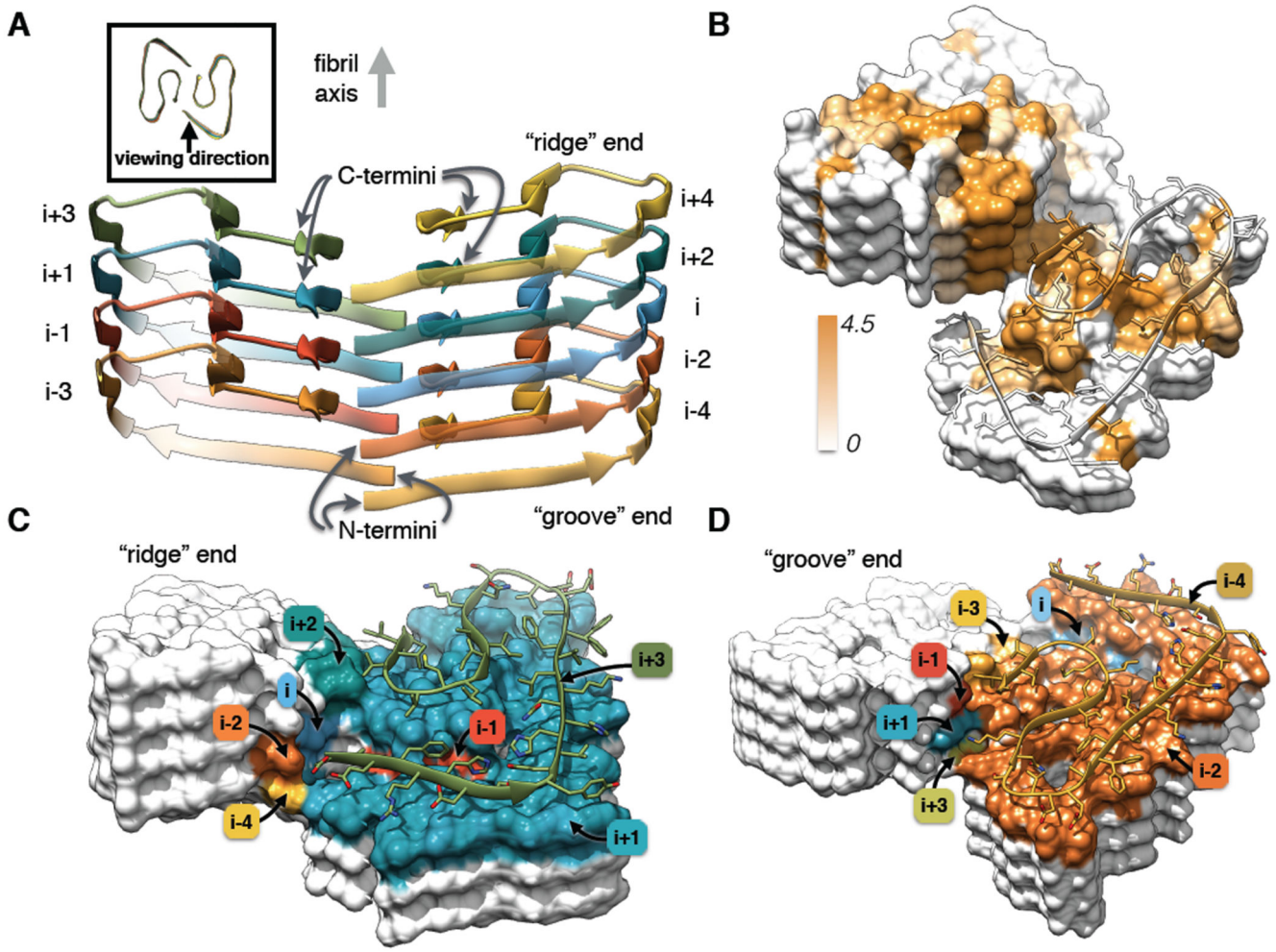

Fig. 4. Details of the Aβ(1-42) fibril architecture.

(**A**) Side view of the atomic model showing the staggered arrangement of the non-planar subunits. (**B**) Surface representation of a fragment of the atomic fibril model. Surface is colored according to hydrophobicity (Kyte-Doolittle scale) (gradient from brown (hydrophobic, 4.5) to white (neutral, 0.0)). View of the "ridge" (**C**) and "groove" (**D**) fibril ends. Only the contact surfaces of the subunits with the respective capping monomer (*i*+3 in (**C**) and *i*-4 in (**D**), shown as ribbon) are colored (color coding according to layer number, see (**A**)).